# Effect of topology changes on the breakup of a periodic liquid jet

Alberto Roman Afanador, Stéphane Zaleski, Gretar Tryggvason, Jiacai Lu

# Effect of topology changes on the breakup of a periodic liquid jet

Alberto Roman Afanador[1], Stéphane Zaleski[2], Gretar Tryggvason[3] and Jiacai Lu[3]

[1] *University of Notre Dame, Notre Dame, IN, USA*

[1] *Sorbonne Université, CNRS and IUF,*

*Institut Jean Le Rond d'Alembert, Paris, France*

[3] *Johns Hopkins University, Baltimore, MD, USA*

(Dated: June 10, 2021)

## Abstract

The breakup of a periodic jet is examined computationally, using a front-tracking/finite-volume method, where the interface is represented by connected marker points moving with the fluid, while the governing equations are solved on a fixed grid. Tracking the interface allows control of whether topology changes take place or not. The Reynolds and Capillary numbers are kept relatively low ($Re = 150$ and $Ca = 2$) so most of the flow is well resolved. The effect of topology changes is examined by following the jet until it has mostly disintegrated, for different "coalescence criterion," based on the thickness of thin films and threads. The evolution of both two-dimensional and fully three-dimensional flows is examined. It is found that although there is a significant difference between the evolution when no breakup takes place and when it does, once breakup takes place the evolution is relatively insensitive to exactly how it is triggered for a range of coalescence criterion, and any differences are mostly confined to the smallest scales.

## I. INTRODUCTION

In single phase flows, direct numerical simulations, or DNS, generally refer to large scale numerical simulations where governing equations believed to describe a particular physical process well, are accurately solved for a turbulent flow with a large range of temporal and spatial scales. Similar simulations have also been done for multifluid and multiphase flows, but almost exclusively for disperse flows where bubbles and drops do not breakup or coalesce (undergo topology changes) [4, 28, 31]. The challenge of doing DNS for flows where the topology of the interface changes is two-fold. First of all is accuracy. The general assumption that DNS results are independent of all numerical parameters, including the resolution, is difficult to maintain during topology changes since films and filaments can become very thin before breaking. Secondly, coalescence usually takes place when a thin film ruptures and the rupture is triggered by short range attractive force that are not included in the modeling since they act at scales that are usually not resolved. Thus, unlike simulations of flows containing clean bubbles or drops, simulations of the breakup of fluid jets are not DNS according to the definition in the first sentence. However, the results of such simulations appear to reproduce reasonably well what is seen experimentally and most of the flow is well resolved so we can probably refer to such simulations as "almost" DNS.

A large number of simulations of the breakup of fluid masses have focused on the atomization of liquid jets. Some of the earliest simulations of fully three-dimensional jets include [2, 3], who used a Volume-of-Fluid (VOF) method, [7, 22, 32, 37], who used level set/ghost fluid methods, and [1, 24, 33], who used hybrid level set/ghost fluid/VOF methods. Studies have included laminar flows [37], turbulent flows [32] and Large Eddy Simulations (LES) with a subgrid model [2, 14, 15]. [6] noted that initial instabilities of the atomization may occur at the subgrid level of an LES and proposed closure models. Instabilities and ligament formation have also been examined in two layer flows [53] and jets in crossflow [16, 36]. As the flow evolves, and instabilities grow, structures with a wide range of length scales emerge, making it difficult to fully resolve the flow, even on modern computers [11]. The formation and breakup of ligaments and droplets is very complex [42–44] and resolving the smallest drops can become computationally expensive. To simulate this multi-scale behavior without increasing the spatial resolution several authors have coupled simulations that resolve most of the flow with Lagrangian Particle methods to represent small droplets [17, 18, 49]. Studies

of the interactions between droplets, ligaments and turbulence, using almost fully resolved flows, have been examined by a number of authors [45, 46]. A review of early simulations of atomization can be found in [11] and for recent papers reporting simulations of atomization see, for example, [13, 26, 27, 40].

Most of the simulations of flows undergoing massive topology changes referenced above have been done using numerical methods where the governing equations for both fluids are solved on a fixed structured grid and a marker function, identifying the different fluid, is advected on the fluid grid using Level-Set or Volume-of-Fluid methods. When those methods are used, topology change takes place when the thickness of a film or a filament is of the order of the mesh size and as the grid is refined, topology change is delayed. Thus, the effect of topology change cannot be separated from the grid resolution.

Instead of directly advecting the marker function on the fixed grid, it is also possible to track the the interface by moving marker points and construct the marker function from the location of the interface. In this case topology changes will only take place if they are explicitly included. We note, however, that even if the interface is retained, once flow structures such as thin films and drops are small enough, the flow will be under-resolved. In early simulations of the breakup of jets by the front-tracking/finite-volume method used here (see [48] for simulations of two-dimensional flows and [47, 50] for three-dimensional flows), topology changes were not included so drops were connected to the main body of liquid by a thin filament. In three dimensions this filament collapsed to a string of points that did not seem to be of much dynamic significance. Recently we have examined much more complex flows using a topology change algorithm coupled with a front-tracking/finite-volume method [29, 30] and studied briefly the impact of varying the criterion for topology change on the overall flow evolution. Here, we examine how topology changes impact the evolution of a periodic jet, comparing the evolution when no topology changes take place with flows where the topology changes.

## II. NUMERICAL METHOD

We consider two- and three-dimensional immiscible jets of heavy fluid moving inside a lighter one in a periodic domain. The flow is governed by the Navier-Stokes equations, which

are written for the whole domain, using the "one-fluid" form:

$$\frac{\partial(\rho\mathbf{u})}{\partial t} + \nabla\cdot(\rho\mathbf{u}\mathbf{u}) = -\nabla p + \nabla\cdot\mu(\nabla\mathbf{u} + \nabla\mathbf{u}^T) + \sigma\int_F \kappa_f \mathbf{n}_f \delta(\mathbf{x}-\mathbf{x}_f)dA_f. \qquad (1)$$

Here, $\mathbf{u}$ is the velocity vector, $\rho$ and $\mu$ are the discontinuous density and viscosity fields, respectively, and the singular last term is the surface tension, which is concentrated at the fluid interface. $\sigma$ is the constant surface tension, $\delta$ is a two or three-dimensional delta function constructed by repeated multiplication of one-dimensional delta functions, $\kappa_f$ is the mean curvature in 2D and twice the mean curvature in 3D, $\mathbf{n}_f$ is a unit vector normal to the front, $\mathbf{x}$ is the point at which the equation is evaluated, and $\mathbf{x}_f$ is a point on the interface. The flow is assumed to be incompressible so the momentum conservation equations are supplemented by the incompressibility condition $\nabla\cdot\mathbf{u} = 0$, which leads to a non-separable elliptic equation for the pressure.

The Navier Stokes equations are solved on a regular structured staggered grid using a second-order predictor-corrector method, the advection terms are approximated using a QUICK scheme and the viscous terms are discretized by second-order centered differences. The different fluids are identified by a marker function ($H = 1$ in the jet fluid and $H = 0$ in the ambient fluid) that is used to set the density and viscosity. The fluid interface is tracked by connected marker points (the "front") to update the marker function and to compute the surface tension. The front points are connected into an unstructured surface grid that is advected by the fluid velocity, interpolated from the fixed grid. As the front stretches and deforms, surface markers are dynamically added and deleted as needed. The surface tension is represented as a singular distribution (delta-functions) at the front. The gradients of the marker function (delta functions when the change is abrupt across the interface) and the surface force are transferred to the fixed grid by approximating them by compact but smooth functions. After the front has been advected, the marker function is reconstructed by integration of the smooth grid-delta function, the density and the viscosity fields are determined from the marker function, and the surface tension added to the nodal values of the discrete Navier-Stokes equations. The method is not completely volume conserving and we therefore sometimes do a global adjustment of the volume by moving the interfaces slightly in the normal direction. In all cases these adjustments are very minor. For disperse flows with bubbles or drops on parallel computers the front can easily be distributed to the different processors, but for continuous interfaces doing so is more complex and here

we simply use a separate processor to update the front. The method, usually referred to as a finite-volume/front-tracking method, was introduced in [52] and is described in detail in [51]. Implementation of similar ideas by other researchers can be found in [4, 8–10, 12, 20, 34, 41, 54, 56], for example.

Topology changes in multiphase flows happen when thin films rupture and slender threads break. Thin threads that break are easier since the Navier-Stokes equations predict that the diameter of threads becomes zero in a finite time and no additional physical modeling needs to be included. The breakup also takes place rapidly and while the thread may be under-resolved just before it breaks, the short time usually ensures that it does not have a significant effect on the overall dynamics of the flow. Most numerical methods designed to handle multiphase flows handle thread breakup easily. Thin films are more challenging. Their thickness is not predicted to go to zero in a finite time by the standard Navier-Stokes equations so additional physics needs to be included to model the rupture. This physics is usually short range attractive forces that make the film go unstable and form a hole that then grows by capillary forces and additional ruptures. These short range forces are generally not included in simulations of multiphase flows. This may, however, not be the only way holes are generated since breakup can also by triggered by perturbations such as particles or bubbles. For an extended discussion of the many ways holes can be formed, see [35].

In the simulations presented here, topology change is accomplished by reconnecting fronts that are closer than a prescribed minimum distance, $\Delta c$. The algorithm consists of two steps: Finding close front points and then restructuring the front: The identification of close points can be done in many ways, but here the domain is divided into sub-domains and a linked list of points in each domain constructed, so that the search can be limited to points in each subdomain. Once close points have been identified, all close points are merged and elements between merged points eliminated. For a short description of a topology change algorithm for front tracking and a few examples see [38].

While we track the interface explicitly using connected marker points, and construct the marker function from the location of the interface, in most other approaches—such as VOF or Level Set methods—the marker function is represented and advected directly on the fixed grid used to solve the flow equations. Those methods will produce topology change when the resolution of a film or a thread is comparable to the grid spacing, and in simulations by these methods rupture takes place when a film is no longer resolved. In many cases

the results look "plausible," but in other cases the grid dependency of the rupture prevents convergence under grid refinement. In VOF methods the marker function is conserved so thin filaments with a thickness of the order of the mesh usually break into droplets, but in level set methods such thin filaments disappear. A few authors have examined how these methods handle breakup and the resulting small small scales using the advection by prescribed velocity fields of circles in two-dimensions and spheres in three-dimensions (for a recent reference see [5]). There have been attempts to improve the capability of methods advecting the marker function on the grid to capture small scales more accurately. In [21] a moment method is used to capture thin under-resolved filaments for two-dimensional flows, and in [19] the marker function is advected using a level set method on a grid that is finer than the grid used for the fluid equations. When the interface is explicitly tracked, thin filaments retain their integrity, even if the velocity field may be under-resolved. We note that for interface tracking by connected markers, as done here, the default behavior is no rupture and if rupture is desired, that must be explicitly added to the method.

## III. PROBLEM SETUP

The computations are done in a rectangular quadrilateral (2D) or a rectangular cuboid (3D) with periodic boundary conditions in one direction (referred to as the horizontal direction), where the jet crosses the periodic boundaries. In 2D it is bounded by two perturbed horizontal interfaces and in 3D the jet is a horizontal perturbed cylinder. The setup is governed by the diameter of the jet and its initial velocity, the material properties of the jet and the surrounding fluid, and surface tension. The overall dimensions of the domain, such as its length, $L$, and height and width, may also influence the results, but here we will assume that those are of secondary importance. For a flat interface between two fluids, subject to shear determined by the jump in velocity, $\Delta U$, and perturbed by sufficiently wide range of modes, the wavelength that grows is selected naturally by the properties of the fluids. Thus, the governing nondimensional numbers are the Capillary number and the ratios of the material properties. For our case the diameter of the jet is also important, giving a Reynolds number. The problem is therefore described by:

$$Ca = \frac{\mu_j \Delta U}{\sigma}; \qquad Re = \frac{\rho_j D \Delta U}{\mu_j}; \qquad r = \rho_j/\rho_f; \qquad m = \mu_j/\mu_f. \tag{2}$$

Here, $\mu_j$, $\rho_j$ are the viscosity and the density of the jet, respectively, $\mu_f$, $\rho_f$ are the viscosity and the density of the surrounding fluid, and $\sigma$ is the surface tension.

For the two-dimensional flow the initial conditions consist of two interfaces perturbed by a random collection of waves

$$y(x) = y_0 + \sum_{n=4}^{10} a_n \Big(\frac{0.03L}{n}\Big) \sin(2\pi x/L + 2\pi b_n), \tag{3}$$

where $a_n$ and $b_n$ are random numbers between 0 and 1 generated by a RAND function. The same set of parameters $(a_n, b_n)$ are used for all the simulations presented here. For the fully three-dimensional flow the radius of the initially cylindrical jet is given by equation (3), and the axis of the jet is given a small perturbation consisting of five waves of amplitude 0.01. The surface tension was selected so that the about six waves consistently grow to a finite amplitude, for various values of the coefficients in equation (3). We note that the growth rate is strongly affected by viscosity and for inviscid flow the most unstable wave number is much higher. Although it is well known that for jets the initial velocity field has important influence on the growth of initial disturbances ([23, 39, 55]), here we simply take the velocity inside the jet to be a constant since the goal is to compare the large amplitude state for different handling of topology changes, rather than reproduce experimental observations. This leads to slight non-divergence at the initial time which is eliminated by the pressure field after the first time step.

The length of the computational domain is $L = 4$ (two-dimensional case) and $L = 6$ (three-dimensional case) in the periodic direction, and the height is equal to 2 for the two-dimensional case and for the three-dimensions case the height and width are 3. The side boundaries are full slip walls. A jet of diameter $D = 0.6$ runs down the middle of the domain. The lighter fluid has density $\rho_f = 1.25$ and viscosity $\mu_f = 0.001$ and the jet fluid has density $\rho_j = 2.5$ and viscosity $\mu_j = 0.01$. The density ratio is therefore $r = \rho_j/\rho_f = 2.0$ and the viscosity ratio is $m = \mu_j/\mu_f = 10$. The surface tension is $\sigma = 0.005$. The initial velocity of the jet is $u_j = 1$ and the ambient fluid is stationary so the velocity jump is $\Delta u = 1$. These values give $Re = \rho_j D\Delta u/\mu_j = 150$ and $Ca = \mu_j \Delta u/\sigma = 2$. The Ohnsorge number is $Oh = \sqrt{Ca/Re} = 0.1155$, which puts the jet well into the "first wind induced break up regime" according to [25] who map the different breakup regimes as functions of $Oh$ and $Re$. Since the density ratio here is relatively small, we expect the effect of the ambient fluid to be more significant than at higher ratios, making the breakup more complex and

closer to the second wind induced regime. We note that the Weber number for the gas, $We = Re\ Ca/r = 150$, is relatively large.

It is obvious that at very large times the phase distributions could look different depending on whether topology changes are included or not. Since an initial velocity is imposed on the jet but no net pressure gradient (or gravity), at long times we expect the velocity to become uniform. If no topology change takes place, the filaments would therefore be pulled back by surface tension and we would end up with a straight jet. If the filaments break and form drops, we are likely to end up with drops and bubbles moving with the flow, unless the drops coalesce before the velocity becomes uniform. We have continued some of our simulations for times much larger than those discussed here and do, indeed, observe that the velocity of the gas and the liquid become the same and the jet is puled back into its original shape. Here, however, we are interested in the relatively early stages of the evolution.

## IV. RESULTS

We start by examining two-dimensional flows, before turning our attention to fully three-dimensional ones. Simulations of two-dimensional flows are much faster and we can therefore gather data for a large number of cases relatively easily, and use finer resolutions.

### A. Two-dimensional flows

Before exploring the effect of topology changes, we examine how fine a grid is needed for convergence and how the initial perturbations affect the evolution. In figure 1, the top left frame shows the effect of the initial perturbation amplitude. The solution is plotted at a relatively early time and while the larger amplitude perturbation grows faster, the same waves grow. The effect of the grid resolution is shown in the right frame where the interface is compared for a simulation on a $128 \times 256$ and on a $256 \times 512$ grid. While there are slight differences, overall the results are very similar. A more quantitative comparison is in the bottom row where the flow rate of the ambient fluid and the interface length are plotted versus time, for four different grid resolutions. Again we see that there are little differences between the results for the three finest grids and almost none for the two finest one. Given that, all the results discussed in this section, for two-dimensional flows, have been computed

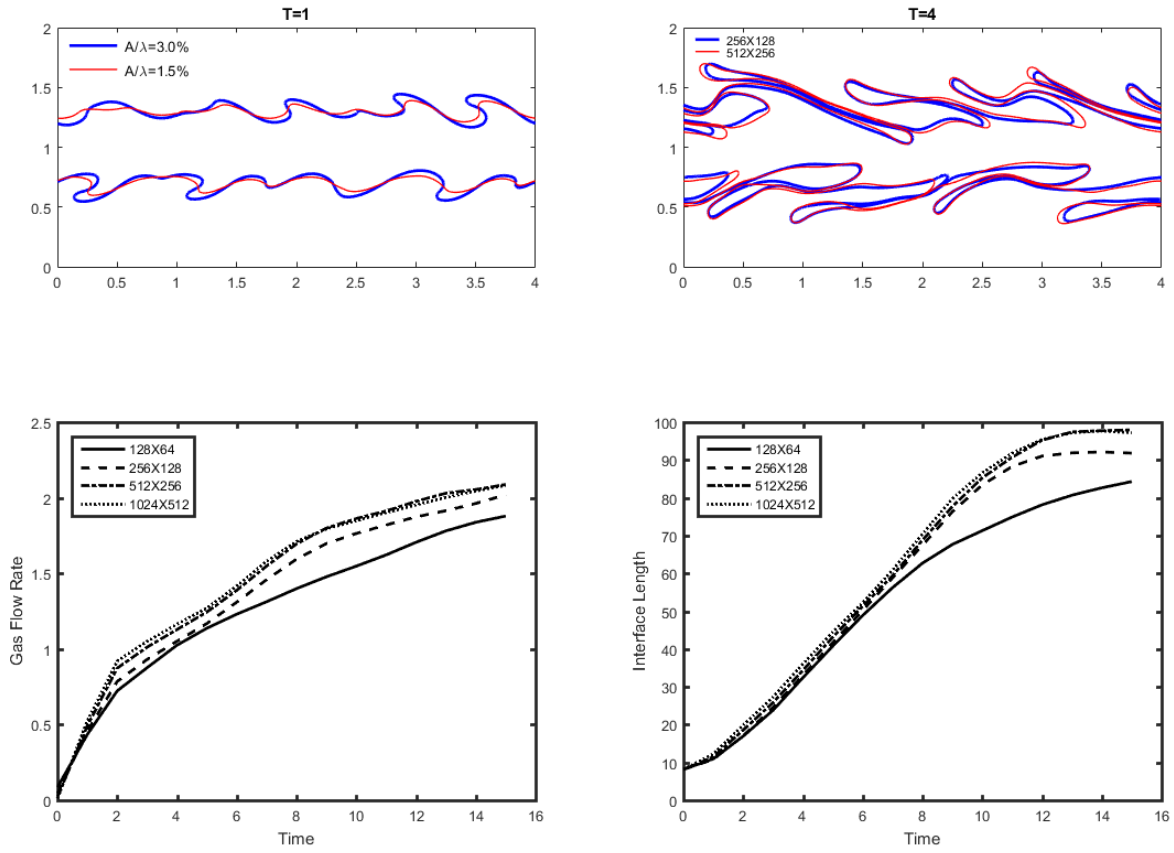


FIG. 1: Effect of the amplitude of the initial perturbation and the grid resolution. See the text for a description of each frame.

on $256 \times 512$ grids, but the much more time consuming simulations of the three-dimension flows in the next section are, however, done using half that resolution ($256 \times 128 \times 128$ grid points).

Figure 2 shows six frames from the evolution of a periodic two-dimensional jet. The interface is shown by a thick line, the vorticity is plotted in the left half of each frame, and the streamfunction in the right half. The first frame shows the initial conditions, where the interface has been perturbed by random waves as discussed above and the velocity inside the jet is constant (the streamlines in the figure are found from the vorticity and are therefore not completely straight). In the second frame the perturbations have grown significantly and several filaments, or "fingers," sometimes with a bulbous head, have been pulled out from from the jet. Surface tension prevents the Kelvin-Helmholtz roll-up seen for single phase flows and the density difference biases the evolution so we see more thin filaments of

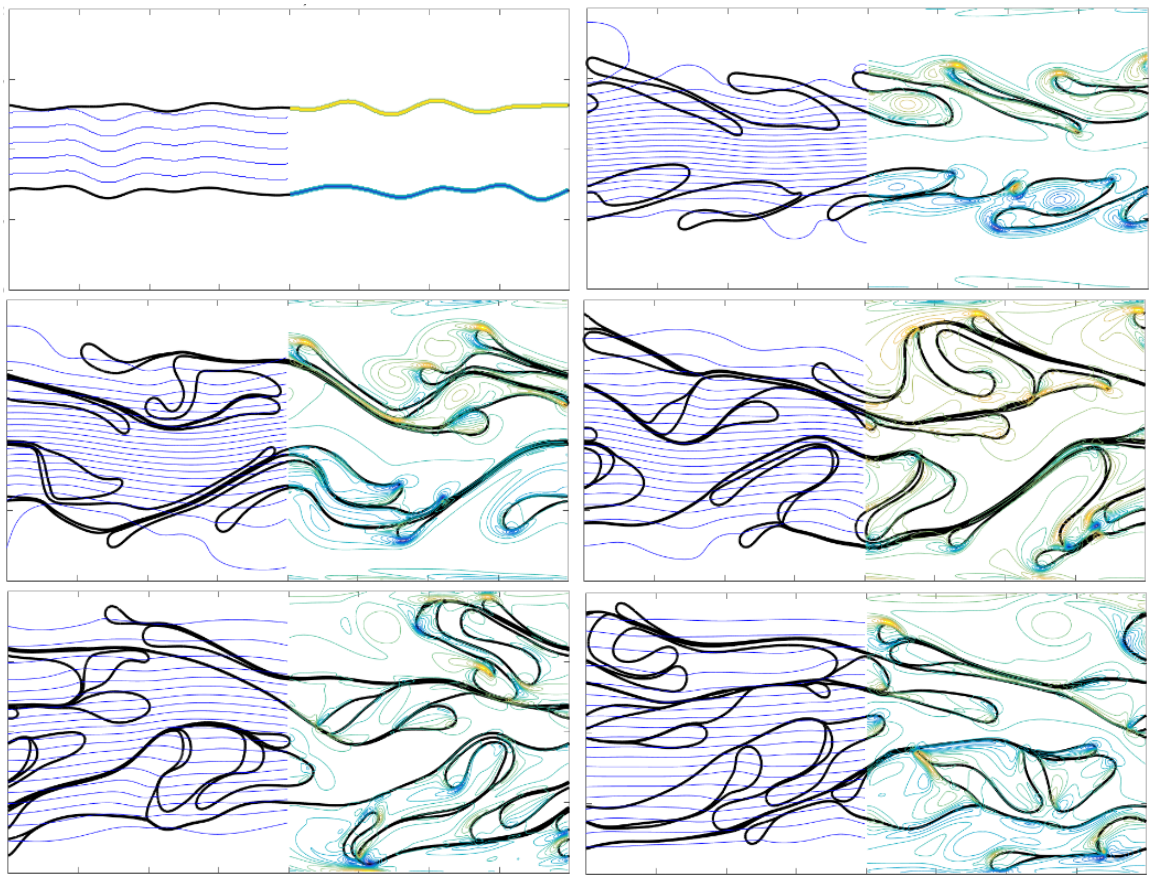

FIG. 2: The two-dimensional jet at time 0.0, 3.0, 6.0, 9.0, 12.0 and 15.0, for no topology changes. In each frame the streamfunction is shown on the left and the vorticity on the right.

the heavy fluid [48] than the light one. In the third frame the original jet starts to meander, but fluid is pulled into filaments in the later frames faster than the large scale meandering can grow, and in the subsequent frames the filaments meander and collide with each other and the original jet, sometimes enclosing blobs of the light fluid. In the last frames many of the fingers have become sufficiently long so that large portions have collapsed into very thin filaments and it does not seems unreasonable to assume that some of them might break. Although the shear is reduced with time as the velocity becomes more uniform, we do not see significant retraction of the long filaments by surface tension, but that is seen if the simulations are continued further.

In figure 3 we show results from three simulations with coalescence at two times, along with results from the simulation in figure 2 at the top (the top right hand frame is the same as the bottom left frame in figure 2). In the second row from the top the coalescence criterion

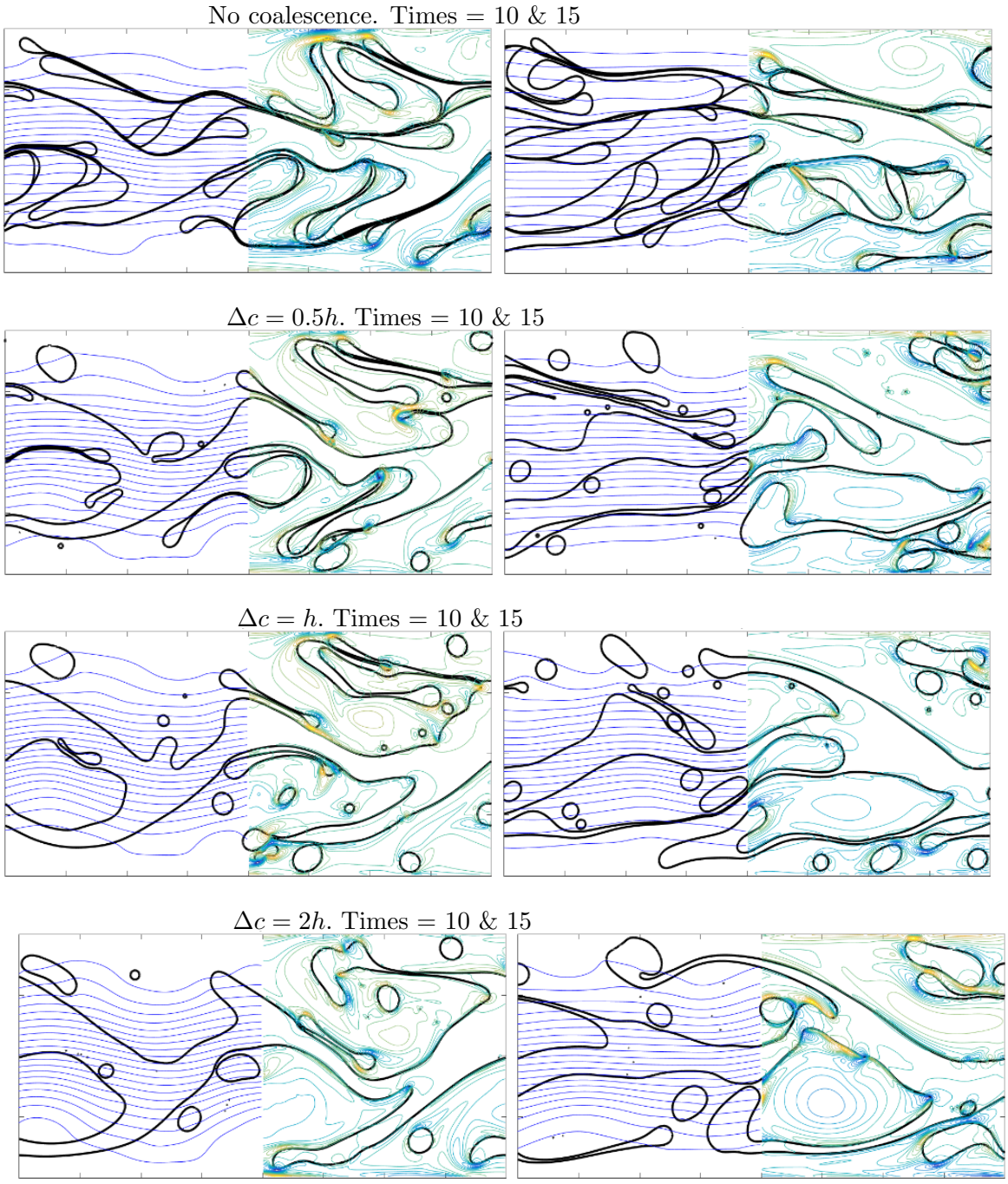


FIG. 3: The two-dimensional jets at times 10 and 15 for topology changes and for $\Delta c = 0.5h,\ h$, and $2h$.

is equal to half the grid spacing ($\Delta c = h/2$), in the third row it is equal to the grid spacing ($\Delta c = h$) and in the bottom row it is equal to twice the grid spacing ($\Delta c = 2h$), where $h$ is the grid spacing. All simulations are started with the same initial perturbations and since coalescence does not take place until large fingers have been formed, the evolutions is the

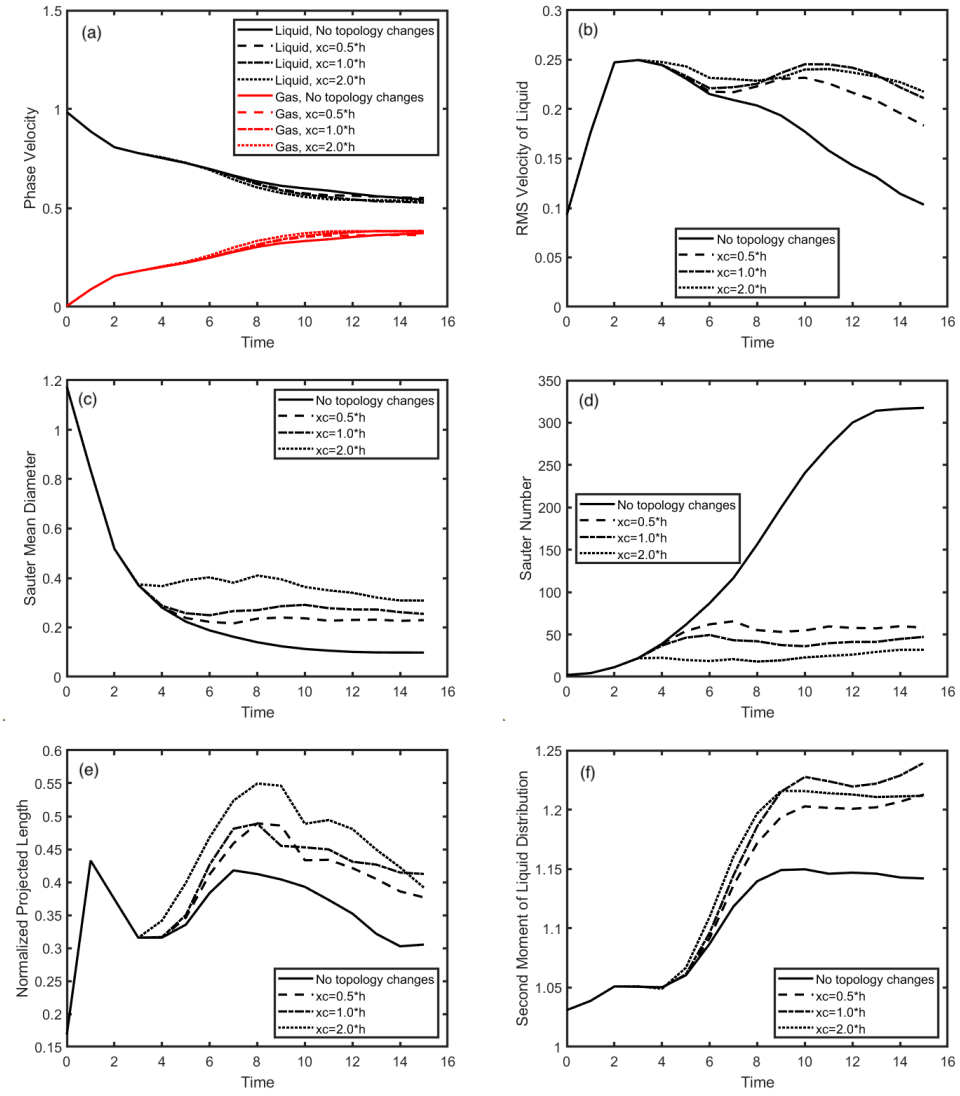


FIG. 4: Several integral quantities versus time for all four two-dimensional jets. (a) Flow rate of lighter (ambient) fluid; (b) RMS velocity of the heavier (jet) fluid; (c) $D_{SM}$: The diameter of the equivalent drops of the heavy fluid (Sauter mean diameter); (d) $N_{SM}$: Number of equivalent drops of the heavy fluid; (e) The horizontal projection of the interface area, normalized by the total area; (f) Second moment of the liquid distribution.

same up to times 3–4, depending on the exact value of the coalescence criterion. Although the overall evolution is similar, particularly for rows two and three, the details are clearly different. For the smallest coalescence criterion (second row), we see several drops of the heavy fluid that have been formed when the fingers break, and although most of the drops are relatively large, a few smaller drops can be seen. Only one (time 10) or two (time 15)

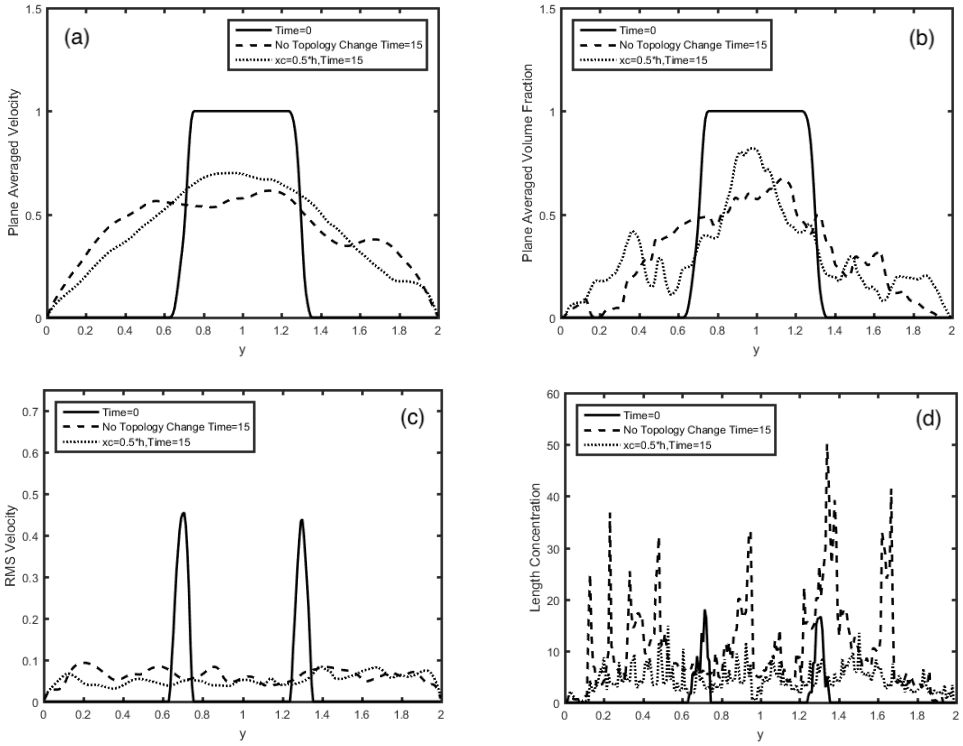


FIG. 5: Profiles of several quantities integrated across horizontal planes for the non-coalescence two-dimensional jet and the $\Delta c = 0.5h$ case at times zero and 15. (a) Horizontal velocity; (b) Volume fraction of heavy fluid; (c) RMS velocity; (d) Area concentration.

bubbles of the lighter fluid inside the heavier fluid can be seen. Although many filaments have broken up into drops, several long filaments can still be seen, particularly at the later time. As the distance at which coalescence takes place is increased to be equal to the grid spacing (row three), we see more drops and some of the remaining filaments are slightly shorter, but not by much. Bubbles of light fluid inside the heavier one remain small and few. When the coalescence distance is further increased to two grid spacings we see fewer drops. This is perhaps somewhat surprising since we expect coalescence to take place more easily. An examination of the evolution at earlier times shows that relatively large drops are formed earlier than in simulations with smaller coalescence distance, but that these large drops quickly merge with the jet again.

In figures 4 and 5 we examine the evolution and the differences between the different cases in more quantitative ways. Figure 4 shows several measures of the evaluation versus time. In frame (a) we plot the average velocity of thee heavy jet fluid (black) which decreases with

time, as well as the average velocity of the light fluid (red), which is "pulled" along with the heavy fluid in the jet. The average velocities converge and eventually we would expect them to become equal. The average velocities are relatively insensitive to the breakup criterion, except for the most aggressive breakup where they converge slightly faster at late times. Frame (b) shows the RMS velocity fluctuations in the heavy fluid. Again, we see relatively small differences between the different cases that break up but the fluctuations are smaller at late time for the case that does not break up. Notice that breakup does not start to take place until after around time 3 (depending on the breakup criterion) so we expect all the cases to be identical until about that time. In frames (c) and (d) we quantify the length of the interface relative to the volume of the jet by computing the Sauter Mean Diameter and the number of equivalent drops by assuming that the heavy fluid is contained in $N_{SM}$ drops with a diameter $D_{SM}$. For two-dimensional flows we denote the total length of the interface by $S$ and the area covered by heavy fluid by $A$, and find that $N_{SM} = S^2/(4\pi A)$ and $D_{SM} = 4A/S$. Frame (c) shows that the $D_{SM}$ is smallest for the non-breakup case and increases as the breakup becomes more aggressive. Similarly, frame (d) shows that $N_{SM}$ is much larger for the non-breakup case than for those where the jet breaks up, as we expect since the interface is much longer, and that the number of equivalent drops then decreases as the breakup becomes more aggressive. In frame (e) we examine if the structure of the interface changes with the breakup criterion by plotting the area projected in the streamwise direction normalized by the total interface length. Again, we see significant difference between the different cases, with the non-breakup case having the smallest value, mainly because the interface is longest there. Finally, frame (f) shows time evolution of the second moment of the heavy fluid, as computed around the jet centerline:

$$M_{2D}^2 = \frac{1}{A_l}\int_V H(x,y)(y-y_c)^2 da; \quad \text{where} \;\; A_l = \int_V H(x,y) da, \tag{4}$$

where $y_c$ is the centerline of the jet. While the jet that does not break does not spread as much as the ones where breakup takes place, there are relatively little differences between the spreading of the breaking jets.

In figure 5 we plot the profiles for a few quantities at the initial time and time 15 for the no-breakup case and the $\Delta c = h$ case. The profiles are found by averaging over planes (or lines, since the flow is two-dimensional) parallel to the walls. Frame (a) shows the average velocity (in both the light and the heavy fluid). The initial velocity for both cases

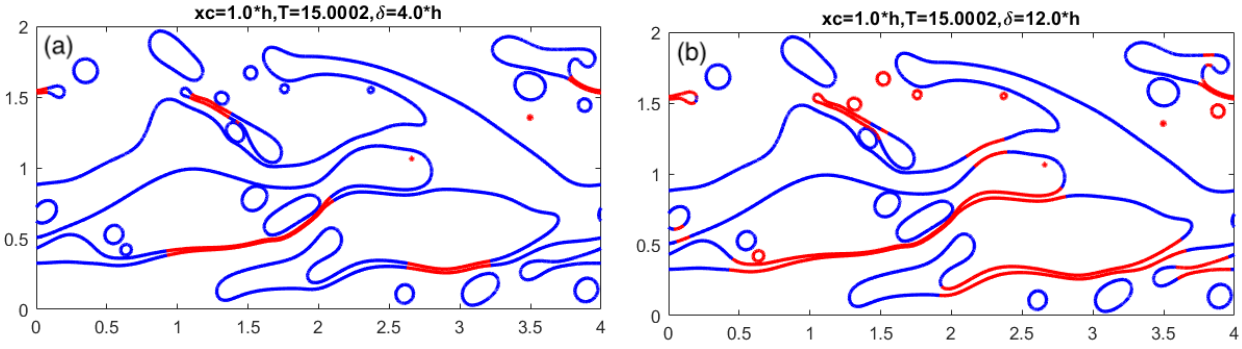


FIG. 6: The interface for the two-dimensional jet at time 15, for $\Delta c = h$. The red curve identifies interfaces bounding small scale fluid structure. In (a) $\delta_{small} = 4h$ and in (b) $\delta_{small} = 12h$.

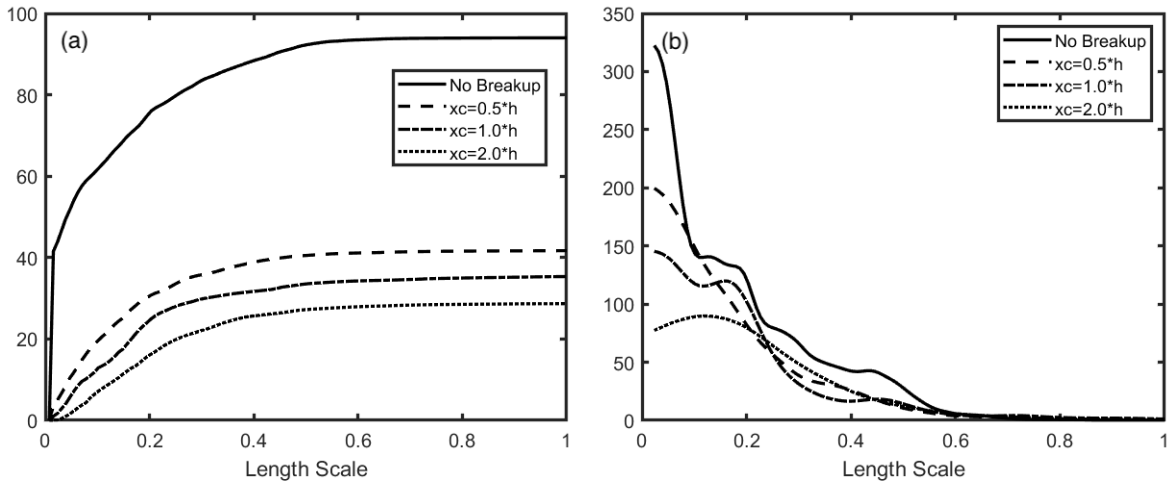


FIG. 7: (a) The cumulative length of interfaces bordering small fluid structures versus the structure size ($\delta_{small}$ as defined in the text), for all four cases, averaged between times 10 and 15. (b) The derivative of the average cumulative distribution for all cases versus the structure size.

is shown by the solid line. While the velocities are similar, it is clear that the velocity for the coalescing jet is more pointed in the middle, while the velocity for the non-coalescing jet is more uniform. The volume fraction for the heavy fluid in frame (b) similarly shows that although relatively similar, the profile for the non-coalescing jet is slightly more uniform in the middle than the coalescing jet, although both show significant fluctuations. The RMS velocity (again, in both fluids) in frame (c) is essentially the same for both cases. In frame (d) we plot the area concentrations and it is clear that although the results fluctuate

significantly, due to the relatively small system being simulated, the no-coalescence case has significantly larger concentration, as expected. The interface area concentration is computed by adding up the interface length falling within grid cells at a specific $y$ location and dividing by the area of all grid cells at this location.

To examine in more detail how breakup and the criterion used to initiate breakup influence the amount of small scale structures of the jet fluid, we first need to identify those. We do so by constructing a normal vector to each interface point and move a given distance, $\delta_{small}$, in the normal direction into the side containing the jet fluid where we interpolate the indicator function from the fixed fluid grid. If the indicator function there is different from what it is in the jet then there is another interface between that point and the interface point we started with. Thus, we identify the interface point as belonging to interface structures smaller than $\delta_{small}$. Generally, interfaces identified with a structure of a given size are also identified with larger size structures, so the total interface length of a given small scale criterion includes the length associated with smaller scales and is therefore cumulative. To get the distribution, we take the derivative of the cumulative distribution. Figure 6 shows the fluid interface at time 15 for a coalescence criterion equal to the grid spacing ($\Delta c = h$), versus the structure size ($\delta_{small}$). In frame (a) the red interface belongs to structures of size $\delta_{small} = 4h$ and in frame (b) it belongs to structures of size $\delta_{small} = 12h$. In both frames the small-scale structures consist of both thin sheets and nearly circular drops, but the larger criterion identifies a larger fraction of the thin films as being small scale as well as most of the small drops.

In figure 7 (a) we show the cumulative length of interfaces bordering small fluid structures versus the structure size ($\delta_{small}$ as defined above), for all four cases, averaged between times 10 and 15. Since the interface where no breakup takes place consists of long and thin filaments, the curve for that case rises sharply for small $\delta_{small}$, and lies above the other cases for all length scales. The total interface length decreases as the coalescence criterion is increased, and while the difference shows up at larger scales, the reason is the different interface length at small scales. Figure 7 (b) show the derivative of the average cumulative distribution for all cases. Since the derivative of the curves in frame (a) results in a fairly noisy distribution, we have smoothed the curves by a Gaussian filter (using matlab with the default smoothing parameter). The interface where no breakup takes place clearly has the largest amount of interfaces bordering small scale structures, and as the breakup criterion

is increased, the amount of small-scale interfaces decreases. The fraction falls gradually to zero as the length scale increases and at the larger scales the difference between the curves is much smaller. Since the system we consider here is relatively small, it is likely that the difference between the curves for the larger scales is not statistically significant and the graph suggests that the amount of interfaces belonging to scales larger than 1.5-2.0 are similar for all four cases.

### B. Three-dimensional flows

Figure 8 shows the interface at three times for a three-dimensional periodic jet that is not allowed to break up. The initial perturbed jet is shown in the first frame. In the second frame the perturbations have grown into folds on the outer edge of the jet. Notice that some of the folds are thicker near the rim so that if holes were to form the edge would become a thread around the jet. The third frame shows that filaments with "bulbous" ends have formed and are bending and meandering with the flow.

The effect of different breakup criteria on the late time interface topology is shown in figure 9 where the interface is plotted at time 15 for the no-breakup case (top) and three different breakup criteria. As for the two-dimensional flows, there is a significant difference between the no-breakup case and the other three. For the parameters simulated here, the jet initially breaks up by forming holes in the folds or sheets that grow from the initial instability. For the smallest criterion the formation of holes is delayed, and initially it has a larger surface area. As more holes form for the larger criterion, the interface becomes more "stringy" and the total surface area keeps increasing as these threads stretch. Finally, the threads break into many smaller drops for the larger criteria, and fewer larger drops for the smallest criterion. Thus, the jet in the second frame from the top consists of filaments and drops of different sizes but in frames three and four from the top the diameters of the drops and filaments are more similar.

Several averaged quantities are plotted versus time in figure 10. The average velocity in the heavy and the light fluids, for different breakup parameter, is shown in frame (a) where it is clear that the breakup criterion does not have a large effect. As the heavy fluid slows down, the light fluid is accelerated but here the process is much slower than for the two-dimensional flows and at the last time shown the average velocity in the light fluid is

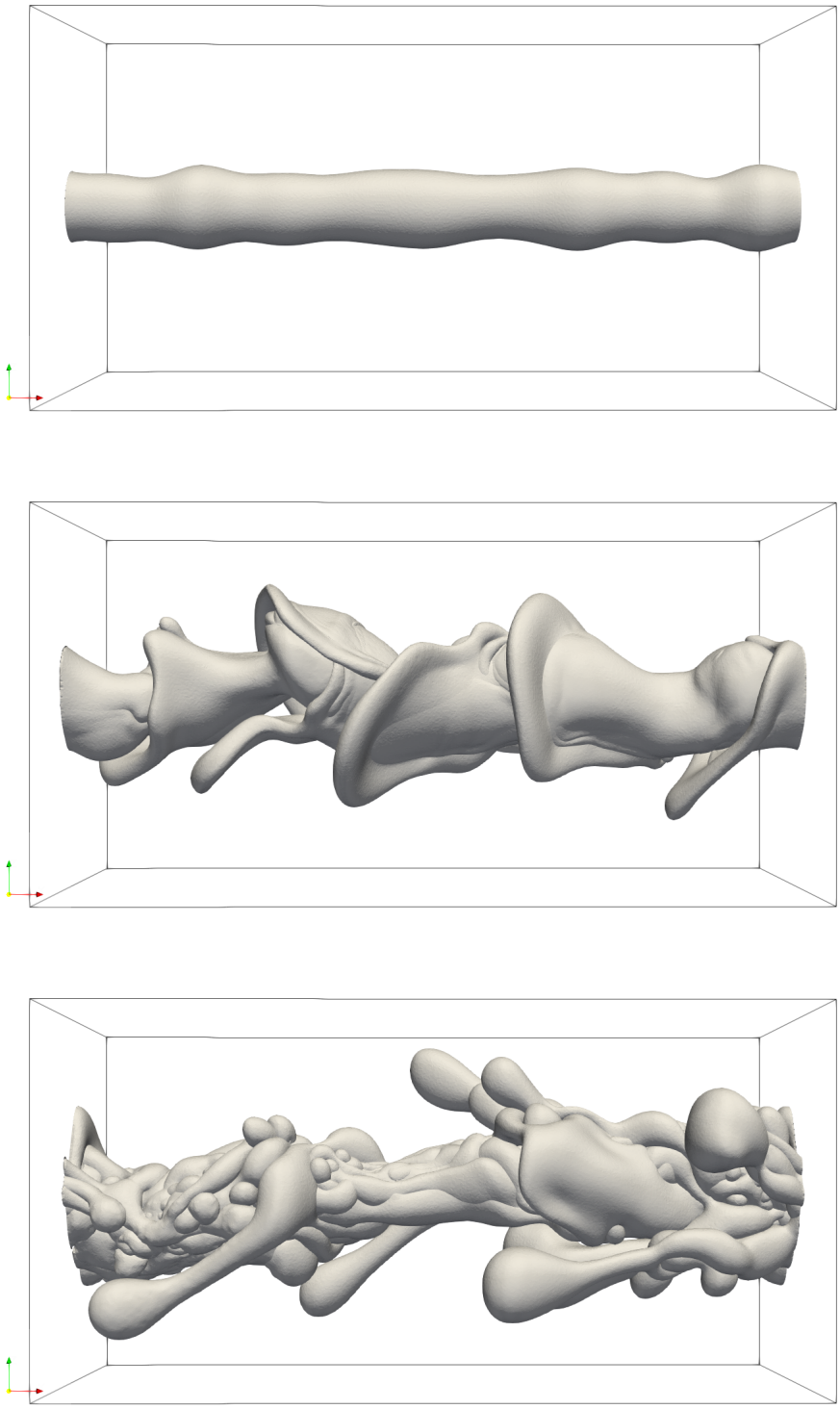

FIG. 8: The interface of the three-dimensional jet at time 0.0, 10 and 20 for a jet with no topology change.

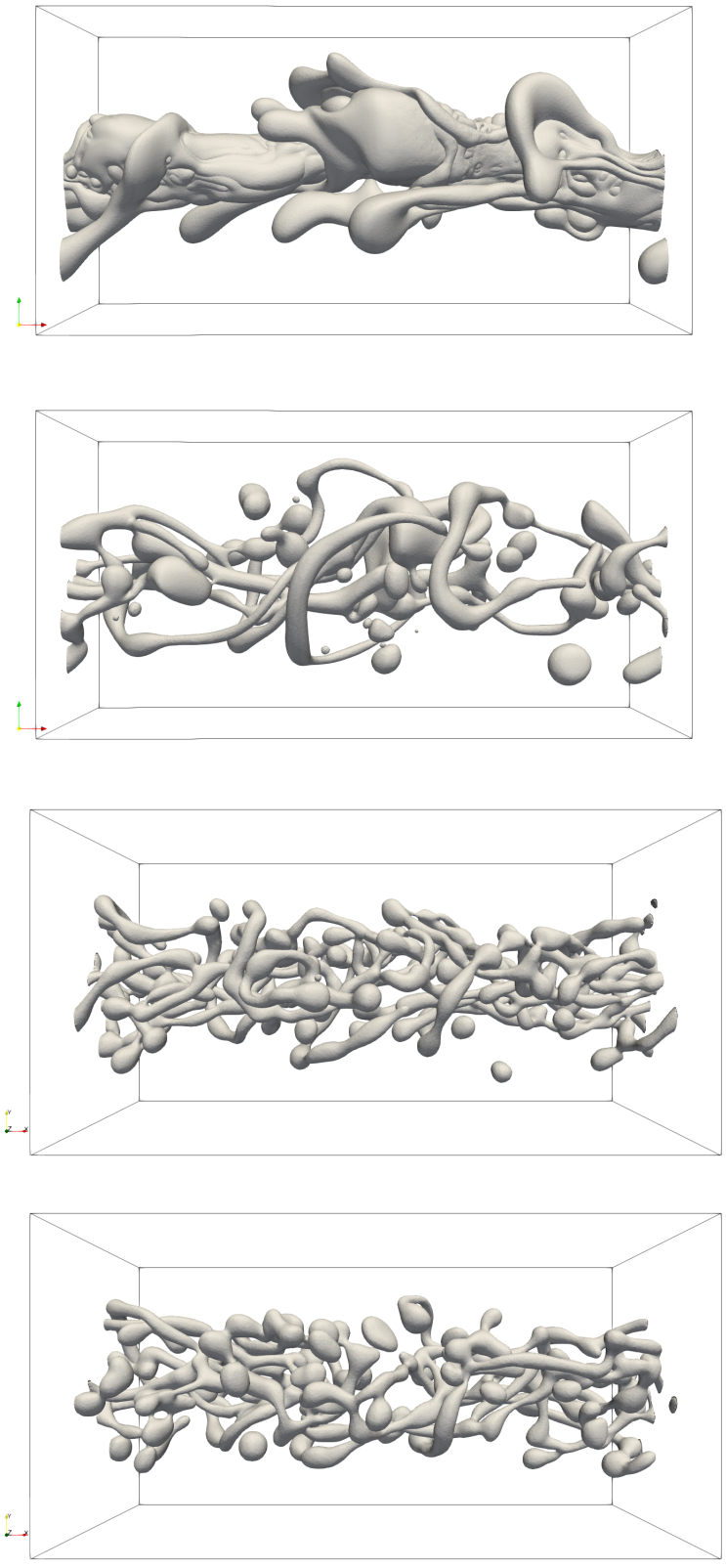

FIG. 9: The interface of the three-dimensional jet at time 15 for no topology change, $\Delta c = 0.32h$, $\Delta c = 0.64h$ and $\Delta c = 0.96h$, respectively.

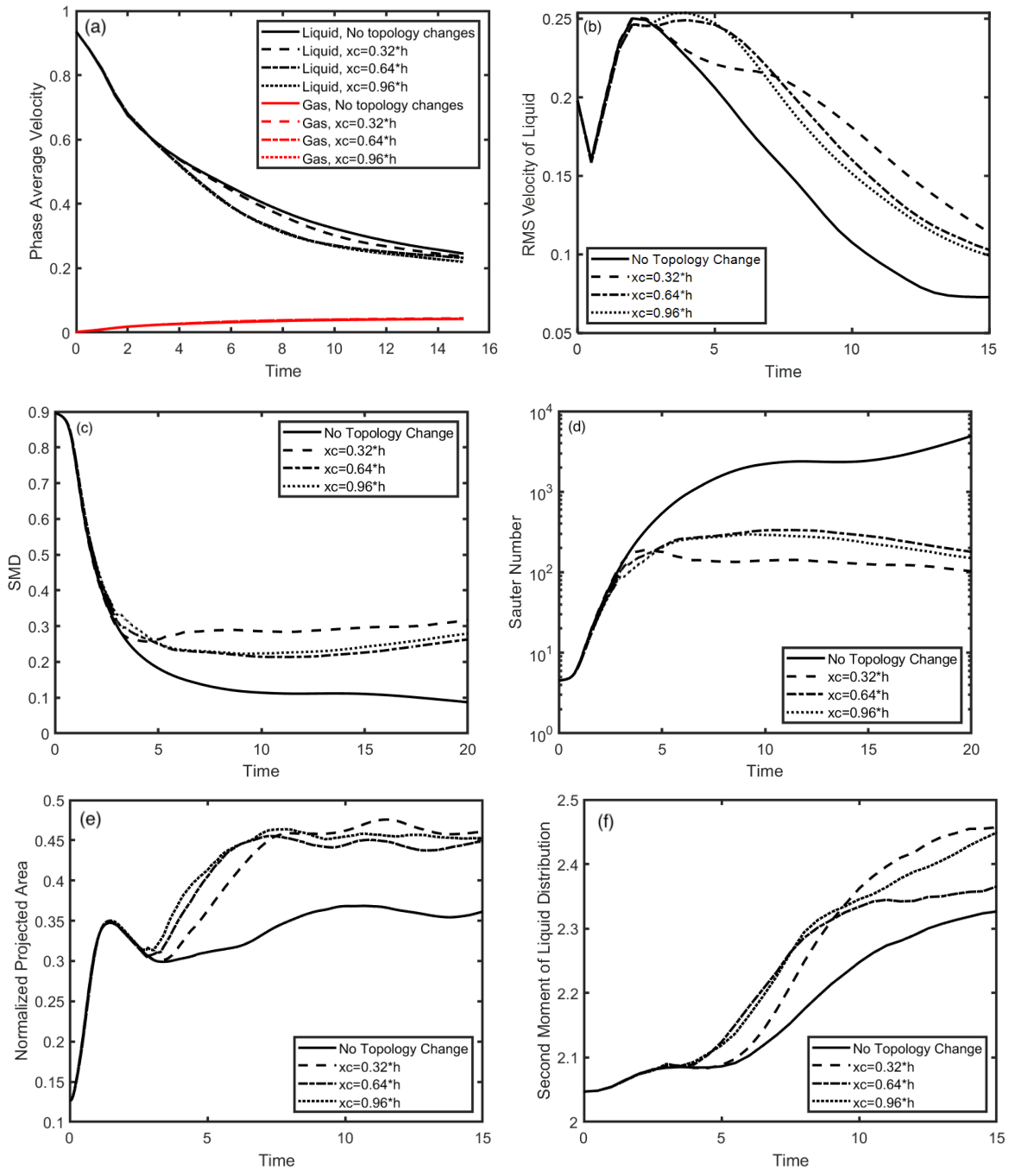


FIG. 10: Several integral quantities versus time for all four three-dimensional jets. (a) Average velocity of the heavier fluid (black) and the lighter fluid (red); (b) RMS velocity of the heavier fluid; (c) $D_{SM}$: The diameter of the equivalent drops of the heavy fluid (Sauter mean diameter); (d) $N_{SM}$: Number of equivalent drops of the heavy fluid; (e) The horizontal projection of the interface area, normalized by the total area; (f) Second moment of the liquid distribution.

only about a fifth of the average velocity in the jet. The volume fraction of the jet fluid is much smaller than for the two-dimensional flows and it is more like a jet in unbounded fluid. Since the domain is finite, however, the velocities in the light and the heavy fluid would eventually become the same if the simulation was continued. The RMS velocity fluctuations are shown in frame (b) and here we see larger differences at late times, just as for the two-dimensional flow. Unlike in two-dimensions, where the fluctuations decrease only for the case without breakup, here the fluctuations decrease for all cases, but most rapidly for the no-breakup case. However, the biggest differences are again between the no-breakup case and the three cases with breakup. The Sauter Mean Diameter and the equivalent number of drops are shown in frames (c) and (d). For a three-dimensional interface with area $S$, enclosing a volume $V$, the Sauter Mean Diameter and the number of equivalent drops that would occupy the same volume are computed by

$$D_{SM} = \frac{6V}{S} \quad \text{and} \quad N_{SM} = \frac{S^3}{36\pi V^2}. \tag{5}$$

The Sauter Mean Diameter is shown on the left, and while the diameter for the no-breakup case is smallest, the results for the other three are similar, although the drops for the smallest criterion are slightly larger than for the other two. The number of equivalent drops is shown in the right frame and we see that for three-dimensional flows the difference in the number of equivalent drops between the case without breakup and the other cases is more dramatic than for the two-dimensional flows. This is partially due to the number being proportional to the cube of the surface area (rather than square as it is for 2D). Notice that the ordinate is logarithmic, thus making the difference between a jet that does not breakup and those that do appear smaller than it actually is. Again, we see that the results for the cases with breakup are similar, but the case with the smallest criterion has the fewest number of equivalent drops. As breakup starts to take place, the simulations with the smallest criterion first follows the no-breakup case for a short time, but then the Sauter Mean Diameter is largest and the number of equivalent drops is smallest for this case. This is because the interface area is smallest and Figure 9 suggest that the reason may be the different sizes of the resulting droplets and possibly the presence of very thin filaments whose area is small. The horizontal projection of the interface area, normalized by the total area, is shown in frame (e). Again we see a significant difference between the no-breakup case and those where breakup takes place. The no-breakup case has the smallest value, but just as for the

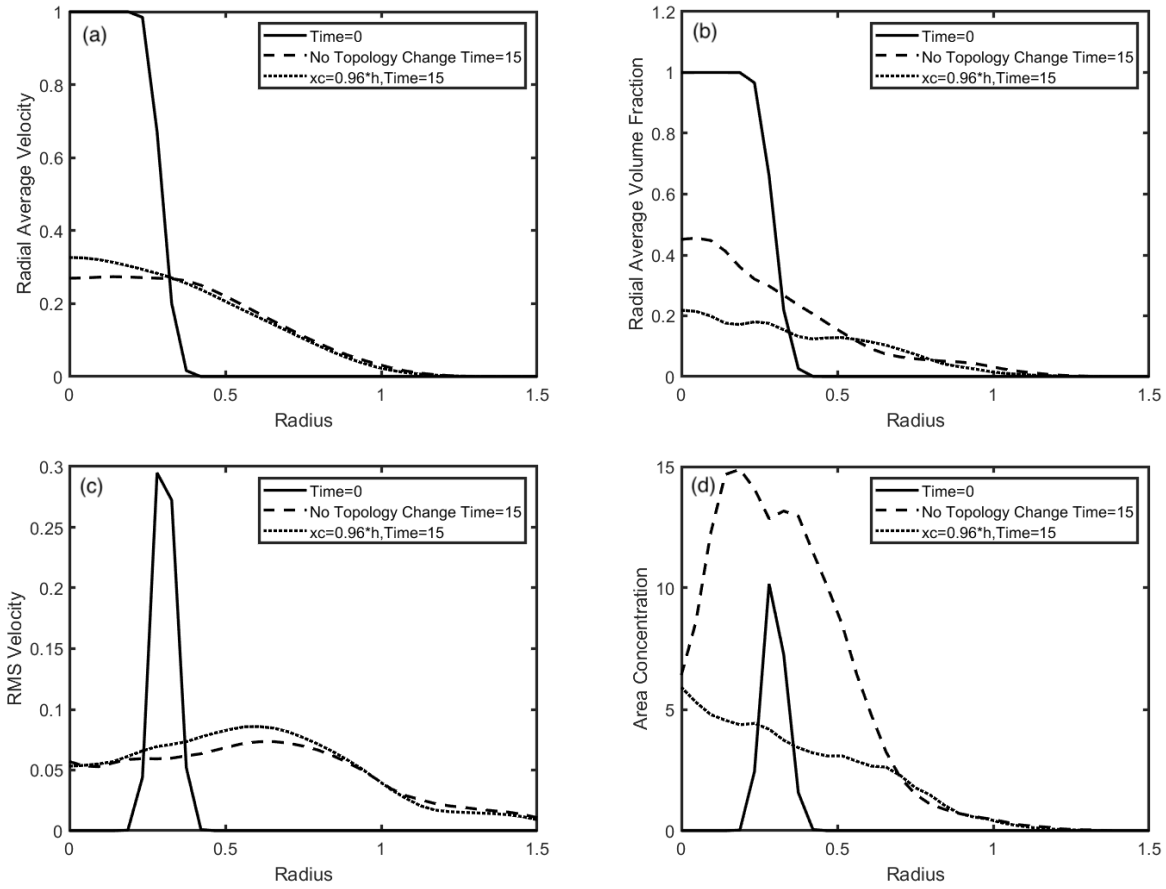


FIG. 11: Profiles of several quantities integrated constant radius cylinders for the non-coalescence three-dimensional jet and the $\Delta c = 0.5h$ case at times zero and 15. (a) Horizontal velocity; (b) Volume fraction of heavy fluid; (c) RMS velocity; (d) Area concentration.

two-dimensional cases, this is mostly because the interface is much longer than for the other cases. The difference between the cases with different breakup criterion is relatively small. The last frame, (f), shows the second moment of the heavy fluid, as computed around the jet centerline, versus time. The second moment is computed in a similar way as for the two-dimensional flow:

$$M_{3D}^2 = \frac{1}{V_l}\int_V H(\mathbf{x})\big(r(\mathbf{x}) - r_c\big)^2 dv; \quad \text{where} \;\; V_l = \int_V H(\mathbf{x}) dv, \tag{6}$$

where $r_c$ is the centerline of the jet. While the jet that does not break does not spread as much as the ones where breakup takes place, there are relatively little differences between the spreading of the breaking jets.

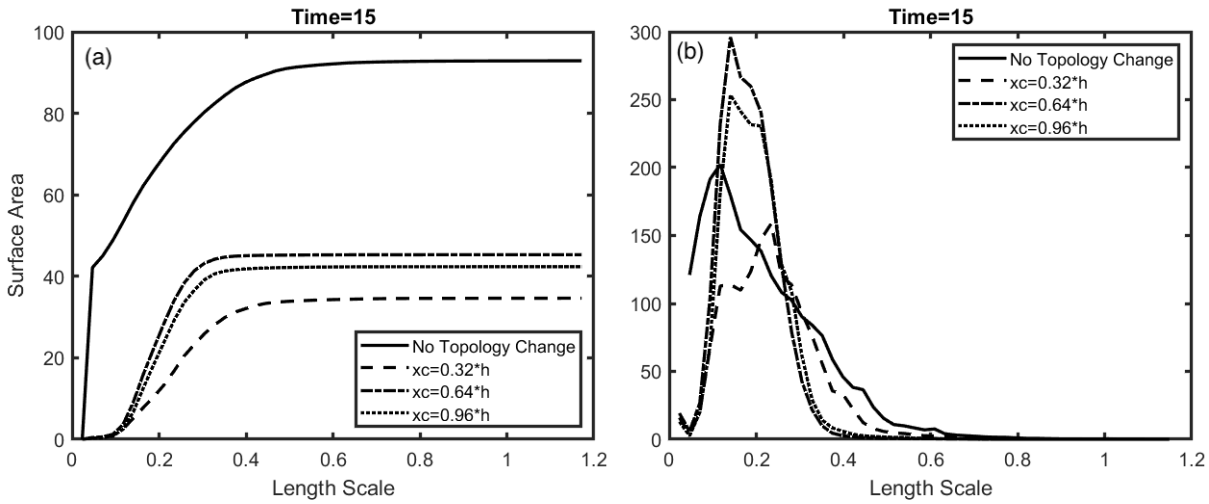


FIG. 12: (a) The cumulative length of the interface versus the scale length at time 15 for the three-dimensional jet. (b) The distribution of interface scales versus the scale length.

In figure 11 we plot the profiles for a few quantities at the initial time and time 15 for the no-breakup case and the $\Delta c = h$ case. The profiles are found by averaging over cylinders centered around the original axis of the jet. Frame (a) shows the average velocity (in both the light and the heavy fluid). The initial velocity for both cases is shown by the solid line. The velocities are very similar, except that the velocity for the jet that break up is slightly larger at the axis, as we saw for the two-dimensional flows also. The radial profile of the volume fraction of the heavy fluid in frame (b) is, however, different and much more of the heavy jet fluid remains on the axis for the jet that does not break up, whereas the volume fraction of the jet that breaks up is more uniform. The RMS velocity in both fluids in frame (c) is essentially the same for both cases. The radial profiles of the area concentration in frame (d) are very different and the area concentration of the jet that does not breakup is much larger and the maximum is slightly off the center axis, whereas the area concentration for the jet that breaks up is largest at the centerline. The interface area concentration is computed by adding up the interface area falling within grid cells at a specific radial location and dividing by the volume of all grid cells at this location.

In figure 12 (a) we show the cumulative length of interfaces bordering small fluid structures versus the structure size computed in the same way as for the two-dimensional flow, for all four cases, at time 15. The area is largest for the no-breakup case, but unlike in two dimensions the reduction is not monotonic with an increase in the coalescence criterion.

Indeed, the smallest criterion results in the smallest surface area, as also seen in figure 10 (c) and (d). Figure 12 (b) shows the distribution, found by differentiating the cumulative surface area. Since the cumulative distribution is smooth for the three-dimensional results, no smoothing is needed. The distribution for the no-breakup case is different than for the cases where topology change takes place, but while the curve peaks at smaller scales, here the maximum is smaller than for the cases with $\Delta c = 0.64h$ and $\Delta c = 0.96h$. The curve for the smallest coalescence criterion, $\Delta c = 0.32h$, is different and has a broader and smaller peak than for the other cases. Unlike the two-dimensional flow where the larger scales were fairly similar, here there are larger differences, and the no-breakup case has more interfaces bordering large structures.

## V. CONCLUSIONS

We have examined the temporal evolution of periodic 2D and 3D jets and the effect of including topology changes or not. The emphasis here is on parameter ranges where most of the flow is reasonably well resolved. Topology changes were found to have a relatively small effect on some flow quantities such as the phase average and plane average velocities in both two-dimensional and three-dimensional flows, but the geometry of the interface varies significantly when comparing cases that include topology changes and the one that does not. For both the two-dimensional and the three-dimensional flows the case with no topology changes continues to stretch and results in a large total surface area.

Once topology change takes place, varying the threshold distance at which topology changes generally has less impact than whether topology change takes place or not, particularly for the various average quantities. For two-dimensional flows the general trend was that as the breakup parameter increased, the equivalent number of drops decreases but their mean size increases. This trend was not seen for the three-dimensional flows, where the size and number of drops did not vary monotonically with the breakup parameter used.

On the one hand, the results presented here are encouraging for users of numerical methods that track the phase distribution by advecting a marker function on a fixed grid, such as by volume of fluid or level set methods or their many modern variants, where coalescence and breakup take place once the thickness of films and filaments reaches the grid size, since many aspects of the flow are relatively insensitive to exactly how and when the breakup

takes place. But, on the other hand, our results also show that the smallest scales in the flow do change when the breakup criterion changes, suggesting that it is unlikely that those methods accurately capture the smallest scales. Although the conditions used here to trigger topology changes are artificial, we believe that the general conclusions would also hold for more physics based criterion.

## VI. ACKNOWLEDGEMENT

This research was supported in part by the Consortium for Advanced Simulation of Light Water Reactors, an Energy Innovation Hub for Modeling and Simulation of Nuclear Reactors under U.S. Department of Energy Contract No. DE-AC05-00OR22725. ARA acknowledges fellowship support from the Kinesis-Fernandez Richards Family Fellowship from the University of Notre Dame. We also acknowledge the use of computational resources at the Maryland Advanced Research Computing Center (MARCC).

[1] Arienti, M., Li, X., Soteriou, M., Eckett, C., Sussman, M., and Jensen, R. (2013). Coupled level- set/volume-of-fluid method for simulation of injector atomization. *J. Propul. Power*, 29(1):147–157.

[2] Bianchi, G. M., Minelli, F., Scardovelli, R., and Zaleski, S. (2007). 3D large scale simulation of the high-speed liquid jet atomization. *SAE Tech. Pap*, xx:2007–01–0244.

[3] Bianchi, G. M., Pelloni, P., Toninel, S., Scardovelli, R., Leboissetier, A., and Zaleski, S. (2005). Improving the knowledge of high-speed liquid jets atomization by using quasi-direct 3D simulation. *SAE Tech. Pap*, xx:2005–24–089.

[4] Bois, B. (2017). Direct numerical simulation of a turbulent bubbly flow in a vertical channel: Towards an improved second-order Reynolds stress model. *Nuclear Engineering and Design*, 321:92–103.

[5] Boniou, V., Schmitt, T., and Vié, A. (2021). Comparison oof interface capturing methods for the simulation of two-phase flow in a unified low-Mach framework. *Hal-03241460*.

[6] Chesnel, J., Reveillon, J., Demoulin, F.-X., and Ménard, T. (2011). Subgrid analysis of liquid jet atomization. *Begell House Inc.*, pages 41–67.

[7] Desjardins, O., Moureau, V., Knudsen, E., Herrmann, M., and Pitsch, H. (2007). Conservative level set/ghost fluid method for simulating primary atomization. In *Proc. Annu. Conf. Inst. Liq. Atom. Spray Syst. Am., 20th. ILASS Am.*, volume Pap. 34. Toronto: Inst. Liq. Atom. Spray Syst.

[8] Dijkhuizen, W., Roghair, I., Annaland, M. V. S., and Kuipers, J. (2010a). DNS of gas bubbles behaviour using an improved 3d front tracking model–drag force on isolated bubbles and comparison with experiments. *Chem. Eng. Sci.*, 65:1415–1426.

[9] Dijkhuizen, W., Roghair, I., Annaland, M. V. S., and Kuipers, J. (2010b). DNS of gas bubbles behaviour using an improved 3d front tracking model–model development. *Chem. Eng. Sci.*, 65:1427–1437.

[10] du Cluzeau, A., Bois, G., and Toutant, A. (2019). Analysis and modelling of Reynolds stresses in turbulent bubbly up-flows from direct numerical simulations. *Journal of Fluid Mechanics*, 866:132–168.

[11] Gorokhovski, M. and Herrmann, M. (2008). Modeling primary atomization. *Annual Reviews of Fluid Mechanics*, 40:343–366.

[12] Hao, Y. and Prosperetti, A. (2004). A numerical method for three-dimensional gas–liquid flow computations. *Journal of Computational Physics*, 196:126–144.

[13] Hasslberger, J., Ketter, S., Klein, M., and Nilanjan, C. (2019). Flow topologies in primary atomization of liquid jets: a direct numerical simulation analysis. *J. Fluid Mech.*, 859:819–838.

[14] Hermann, M. and Gorokhovski, M. (2008). An outline of a LES subgrid model for liquid/gas phase interface dynamics. *Proceedings of the 2008 CTR summer program, center for turbulence research*, pages 171–181.

[15] Hermann, M. and Gorokhovski, M. (2009). A large eddy simulation subgrid model for turbulent phase interface dynamics. *11th triennial international annual conference on liquid atomization and spray systems.*

[16] Herrmann, M. (2010a). Detailed numerical simulations of the primary atomization of a turbulent liquid jet in crossflow. *Journal of Engineering for Gas Turbines and Power*, 132:061506 (10 pages).

[17] Herrmann, M. (2010b). A parallel eulerian interface tracking/lagrangian point particle multiscale coupling procedure. *Journal of Computational Physics*, 229(3):745–759.

[18] Herrmann, M. (2011a). The influence of density ratio on the primary atomization of a turbulent liquid jet in crossflow. *Proceedings of the Combustion Institute*, 33:2079–2088.

[19] Herrmann, M. (2011b). On simulating primary atomization using the refined level set grid method. *Atomization and Sprays*, 283–301:21.

[20] Hua, J. and Lou, J. (2007). Numerical simulation of bubble rising in viscous liquid. *Journal of Computational Physics*, 222:769–795.

[21] Jemison, M., Sussman, M., and Shashkov, M. (2015). Filament capturing with the multimaterial moment-of-fluid method. *Journal of Computational Physics*, 285:149–172.

[22] Kim, D., Desjardins, O., Herrmann, M., and Moin, P. (2007). The primary breakup of a round liquid jet by a coaxial flow of gas. In *Proc. Annu. Conf. Inst. Liq. Atom. Spray Syst. Am., 20th. ILASS Am.*, volume Pap. 8. Toronto: Inst. Liq. Atom. Spray Syst.

[23] Klein, M., Sadiki, A., and Janicka, J. (2003). A digital filter based generation of inflow data for spatially developing direct numerical or large eddy simulations. *Journal of Computational Physics*, 186:652–665.

[24] Lebas, R., Ménard, T., Beau, P., Berlemont, A., and Demoulin, F. (2009). Numerical simulation of primary break-up and atomization: DNS and modelling study. *International Journal of Multiphase Flow*, 35:247–260.

[25] Lefebvre, A. (1989). *Atomization and Sprays*. Taylor and Francis.

[26] Ling, Y., Fuster, D., Tryggvason, G., and Zaleski, S. (2019). A two-phase mixing layer between parallel gas and liquid streams: multiphase turbulence statistics and influence of interfacial instability. *Journal of Fluid Mechanics*, 859:268–307.

[27] Ling, Y., Fuster, D., Zaleski, S., and Tryggvason, G. (2017). Spray formation in a quasi-planar gas-liquid mixing layer at moderate density ratios: A numerical closeup. *Physical Review Fluids*, 2:014005.

[28] Lu, J. and Tryggvason, G. (2013). Dynamics of nearly spherical bubbles in a turbulent channel upflow. *Journal of Fluid Mechanics*, 732:166–189.

[29] Lu, J. and Tryggvason, G. (2018). Direct numerical simulations of multifluid flows in a vertical channel undergoing topology changes. *Physical Review Fluids*, 3:084401 (20 pages).

[30] Lu, J. and Tryggvason, G. (2019). Multifluid flows in a vertical channel undergoing topology changes–effect of void fraction. *Physical Review Fluids*, 4:084301.

[31] Ma, M., Lu, J., and Tryggvason, G. (2015). Using statistical learning to close two-fluid multiphase flow equations for a simple bubbly system. *Physics of Fluids*, 27:092101.

[32] Ménard, T., Beau, P.-A., Tanguy, S., Demoulin, F.-X., and Berlemont, A. (2005). Primary break-up: DNS of liquid jet to improve atomization modelling. *Comput. Meth. Multiphase Flow III*, xx:343–352.

[33] Ménard, T., Tanguy, S., and Berlemont, A. (2007). Coupling level set/vof/ghost fluid methods: Validation and application to 3d simulation of the primary break-up of a liquid jet. *International Journal of Multiphase Flow*, 33:510–524.

[34] Muradoglu, M. and Kayaalp, A. D. (2006). An auxiliary grid method for computations of multiphase flows in complex geometries. *Journal of Computational Physics*, 214:858–877.

[35] Néel, B. and Villermaux, E. (2018). The spontaneous puncture of thick liquid films. *J. Fluid Mech.*, 838:192–221.

[36] Pa, M., Pitsch, H., and Desjardins, O. (2009). Detailed numerical simulations of primary atomization of liquid jets in crossflow. *47th AIAA Aerospace Sciences Meeting Including the New Horizons Forum and Aerospace Exposition*.

[37] Pan, Y. and Suga, K. (2006). A numerical study on the breakup process of laminar liquid jets into a gas. *Physics of Fluids*, 18:052101.

[38] Razizadeh, M., Mortazavi, S., and Shahin, H. (2018). Drop breakup and drop pair coalescence using front-tracking method in three dimensions. *Acta Mechanica*, 229:1021–1043.

[39] Sander, W. and Weigand, B. (2008). Direct numerical simulation and analysis of instability enhancing parameters in liquid sheets at moderate reynolds numbers. *Physics of Fluids*, 20:053301.

[40] Schillaci, E., Antepara, O., Balcazar, N., Serrano, J. R., and Oliva, A. (2019). A numerical study of liquid atomization regimes by means of conservative level-set simulations. *Computers & Fluids*, 179:137 – 149.

[41] Shang, X., Luo, Z., and Bai, B. (2019). Numerical simulation of dynamic behavior of compound droplets on solid surface in shear flow by front-tracing method. *Chemical Engineering Science*, 193:325–335.

[42] Shinjo, J. and Umemura, A. (2010). Simulation of liquid jet primary breakup: Dynamics of ligament and droplet formation. *International Journal of Multiphase Flow*, 36:513–532.

[43] Shinjo, J. and Umemura, A. (2011a). Detailed simulation of primary atomization mechanisms in diesel jet sprays (isolated identification of liquid jet tip effects). *Proceedings of the Combustion Institute*, 33:2089–2097.

[44] Shinjo, J. and Umemura, A. (2011b). Surface instability and primary atomization characteristics of straight liquid jet sprays. *International Journal of Multiphase Flow*, 37:1294–1304.

[45] Shinjo, J. and Umemura, A. (2013). Droplet/turbulence interaction and early flame kernel development in an autoigniting realistic dense spray. *Proceedings of the Combustion Institute*, 34:1553–1560.

[46] Shinjo, J., Xia, J., and Umemura, A. (2015). Droplet/ligament modulation of local small-scale turbulence and scalar mixing in a dense fuel spray. *Proceedings of the Combustion Institute*, 35:1595–1602.

[47] Tauber, W. and Tryggvason, G. (2000.). Direct numerical simulations of primary breakup. *Computational Fluid Dynamics Journal*, 9(1):.

[48] Tauber, W., Unverdi, S., and Tryggvason, G. (2002). The nonlinear behavior of a sheared immiscible fluid interface. *Physics of Fluids*, 14:2871–2885.

[49] Tomar, G., Fuster, D., Zaleski, S., and Popinet, S. (2010). Multiscale simulations of primary atomization. *Computers & Fluids*, 39:1864–1874.

[50] Tryggvason, G., Bunner, B., Esmaeeli, A., Juric, D., Al-Rawhai, N., Tauber, W., Han, J., Nas, S., and Jan, Y.-J. (2001). A front tracking method for the computations of multiphase flow. *Journal of Computational Physics*, 169:708–759.

[51] Tryggvason, G., Scardovelli, R., and Zaleski, S. (2011). *Direct Numerical Simulations of Gas-Liquid Multiphase Flows*. Cambridge University Press.

[52] Unverdi, S. O. and Tryggvason, G. (1992). A front-tracking method for viscous, incompressible, multi-fluid flows. *Journal of Computational Physics*, 100:25–37.

[53] Valluri, P., Naraigh, L. O., Ding, H., and Spelt, P. (2010). Linear and nonlinear spatiotemporal instability in laminar two-layer flows. *Journal of Fluid Mechanics*, 656:458–480.

[54] van Sint Annaland, M., Dijkhuizen, W., Deen, N., and Kuipers, J. (2006). Numerical simulation of gas bubbles behaviour using a 3D front tracking method. *AIChE Journal*, 52:99–110.

[55] Wu, P., Miranda, R., and Faeth, G. (1995). Effect of initial flow conditions on primary break-up of nonturbulent and turbulent liquid jets. *Atomization and Sprays*, 5:175–196.

[56] Yamamoto, Y., Higashida, S., Tanaka, H., Wakimoto, T., Ito, T., and Katoh, K. (2016). Numerical analysis of contact line dynamics passing over a single wettable defect on a wall. *Physics of Fluids*, 28:082109.